Graphene Functionalization of Polyrotaxane Encapsulated PEG-based PCMs: Fabrication and Applications

Guang-Zhong Yin, [a, b, *] Xiao-Mei Yang, [b] Alba Marta López, [b] Javier García Molleja, [b] Mei-Ting Wang, [c] De-Yi Wang [a, b, *]

[a] *Escuela Politécnica Superior, Universidad Francisco de Vitoria, Ctra. Pozuelo-Majadahonda Km 1.800, 28223, Pozuelo de Alarcón, Madrid, Spain*

[b] *IMDEA Materials Institute, C/Eric Kandel, 2, 28906 Getafe, Madrid, Spain*

[c] *Shenyang University of Chemical Technology, Shenyang 110142, China*

Corresponding authors

*Tel: +34 91 549 34 22, Email: deyi.wang@imdea.org

*Tel: +34 61 566 44 38, Email: amos.guangzhong@ufv.es

Abstract. In recent decades, phase change materials (PCMs) have received much attention in thermal regulation of electronic devices. But the main limitation for the use of organic PCMs are the low thermal conductivity and leakage during the phase change process. This work will try to improve these limitations, to increase thermal conductivity of the leakage proof PCM formed by a polyrotaxane that serves as a support material to encapsulate PEG 6k. For this purpose, different contents of graphene nanoplatelets (GNP) would be blended. To facilitate its post-industrial production and to meet ecological standards, the synthesis of this PCM is simple and only use water as a solvent. The PCMs can be thermal processed conveniently by hot press. Furthermore, the PCMs created in this work achieves a high thermal performance with high enthalpy values (132.9 -142.9 J/g), due to the action of GNPs as thermal conductive fillers, also experiencing an increase of 60%-257% in thermal conductivity values the higher the GNP content, and also shows

a great shape stability and no leakage during its phase change. These improvements solve the main problems of organic PCMs thus making PLR-PEG-GNP based materials a good candidate to be used as thermal energy storage material in industrial applications as thermoregulator of solid-state disks or realizing the “shaving peaks and filling valleys” effect for thermoelectric generator.

Keywords: Polyrotaxane; Phase Change Materials; Graphene; Nanocomposites; Energy storage

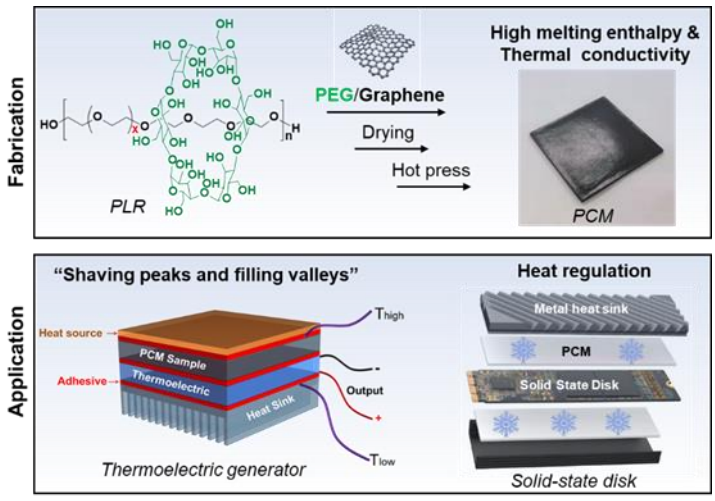

1. INTRODUCTION

In recent decades, with the advancement of the development of technologies and the implementation of 5G, the thermoregulation of devices has become a problem, since they consume more and more energy and therefore generate more heat that must be dissipated if we want the useful life of the devices to be long-lasting, these problems have already been seen in laptops, smartphones, new photovoltaic solar cells, cameras, means of transport and in many others.[1] The use of ecofriendly materials and the development of green energy management materials has become necessary to avoid environmental problems in the future, such as pollution and the depletion of fossil resources and the increase of adverse effects of climate change. [2]

Among the thermal energy storage materials, the phase change materials (PCM) stand out. These materials can store energy in the form of latent heat and release the energy when there is a difference in environmental temperature, this energy exchange occurs when there is a phase change of the material itself.[3] This occurs in an endothermic process, when the temperature of surroundings increases it absorbs energy in a fusion process with collapse of the solid crystalline structure. While when the temperature drops, it proceeds to the crystallization process and the energy is released back to the surroundings.[4] Within the many applications of PCM are: temperature adaptable greenhouses,[5] solar energy storage, [6] cooling of electronic circuitry,[7] building applications, and textile industry, [8] and so on. The main problems of PCMs in general from their commercialization and production are a low thermal conductivity, poor form stability, supercooling, PCM leakage during the phase change that cause failures in the process. [9] Another main problem of PCMs is the difficulty of obtaining flexible PCMs, because many of the prepared materials are rigid or in powder form, which require further

processing for practical applications.[10] In the fields of energy storage and electronic devices are developing to flexible, lightweight, and wearable, so it is required the materials have proper mechanical strength and flexibility.

Within these organic PCMs, polyethylene glycol (PEG) based PCMs are widely used in the fields of solar energy harvesting, [11] waste heat energy recovery, [12] and electric energy storage.[13] Among the properties of PEG are its large phase transformation enthalpy, wide transition temperature, chemical stability, ease of chemical modification, low vapor pressure, low cost, and non-corrosive nature.[14] But like all organic PCMs, they have the same typical drawbacks, which are low thermal conductivity, and leakage during the phase change from solid to liquid.

To generate form stable PEG based PCM composites, there are three common ways: the first is encapsulation of PEG in shell materials.[15] The problem with this technique using PEG as core material is that the highly hydrophilic nature of PEG makes its encapsulation a challenge. Another way would be the preparation of polymer/PEG blending composites, the best known with cellulose diacetate, agarose, chitosan, and various sugars such as glucose, fructose, and lactose.[16-17] In these polymers the intermolecular hydrogen bonding between PEG and hard segment plays an important role towards preventing liquid separation. The most notorious problems of these two methods are their low thermal conductivity, their low latent heat capacities, their incongruent melting and freezing, and complex manufacturing processing. The third method is the impregnation of PEG into inorganic materials with porous or layered structures, such as Graphene [18], Graphene oxide,[19] MXene, [20] Boron nitride, [21] or other carbon based functional fillers.[22] But these inorganic components mean that the more their content grows, the less flexible the

material becomes, in addition to losing energy retention capacity in the form of latent heat.[13]

In the previous report, the Polyrotaxane (PLR) was prepared with simple and green pathway.[10] The form stability at temperatures above the melting temperature of PEO was significantly increased with the addition of α-CD. This new material has good processability and high shape stability, but still suffers from the disadvantages of traditional PCMs (a still low latent heat storage capacity and low thermal conductivity). In this work the PLR was selected as the support materials for PEG based PCMs, this election was decided since the molecular main chain of PLR is almost the same as PEG, that structural similarity ensures the compatibility between PLR and PEG. Furthermore, PLR itself is also a PCM with excellent performance, especially the form stability, that can solve the problems associated with PEG, such as its instability and leakage during phase change. This way solves the most significant problems of the organic PCMs, but the drawback of low thermal conductivity still remains to be solved.

GNPs attracted wide interest, especially in polymer nanocomposites, since their discovery in 2004.[23] As for PCMs, it has been demonstrated that the thermal conductivity has been significantly increased by adding a small amount of GNP content in different PCMs such as palmitic acid [24] or in 1-octadecanol [25] and for our interest in PEG. [26] Therefore, in this work we will try to increase the thermal conductivity of PLR/PEG based PCM by adding Graphene nanoplatelets (GNPs) as a filler. GNPs consists of a two-dimensional lattice of carbon atoms arranged in a honeycomb structure materials with single or multilayers graphite plane.[27] Between their properties we can noted the high thermal conductivity (5000 W/(m K), high specific surface area due to its 2D structure, and excellent Young's modulus, and tensile strength this latter property reported for a single-layer graphene, which nominates this material as the strongest available material.[28]

Also, GNPs appear as an excellent alternative to pristine graphene due to their low cost and the possibility of production on a large scale.[29] Our intention is to increase the PLR-PEG PCMs thermal conductivity with the use of GNP as a filler, for this we will add different GNP content, keeping the synthesis process simple and ecofriendly, only using water as solvent. Also maintaining the excellent properties which already has PLR-PEG such as high form stability and high phase transition enthalpy in order to obtain a material with a high-performance as solid-solid PCM for uses like solar energy storage, and cooling of electronic devices.

2. RESULTS AND DISCUSSION

2.1 Fabrication and structure characterization

We choose PLR-50% with high cyclodextrin content as the support materials (See SI for specific synthesis steps), because based on our previous work, the PLR-50% performed excellent shape stability. Following previous work, we opted for a simple, ecofriendly synthesis process using water as the only solvent. The production of graphene-doped polyrotaxane was fabricated in three steps. First the polyrotaxane was synthesized following the previous work [19]. Then the previously dissolved PEG is mixed with the dissolved and previously sonified GNP, and finally mixed with the polyrotaxane, as shown in **Figure 1a**. Then, through freeze-drying and hot pressing, we can obtain PCM composites with specific shape and size. It is worth pointing out that we choose 150 wt% PEG loading in this paper because it is relatively high in the late heat and maintains certain mechanical properties. When the filling amount is 200 wt% or more, the sample is very easy to brittle fracture (**Table S1**). As shown in **Figure 1**b-d, the sample has excellent plasticity and easily to be hot pressed to get designed shape. And when the thickness of the sample is 1 mm or less, it shows good bending toughness (**Figure 1d**).

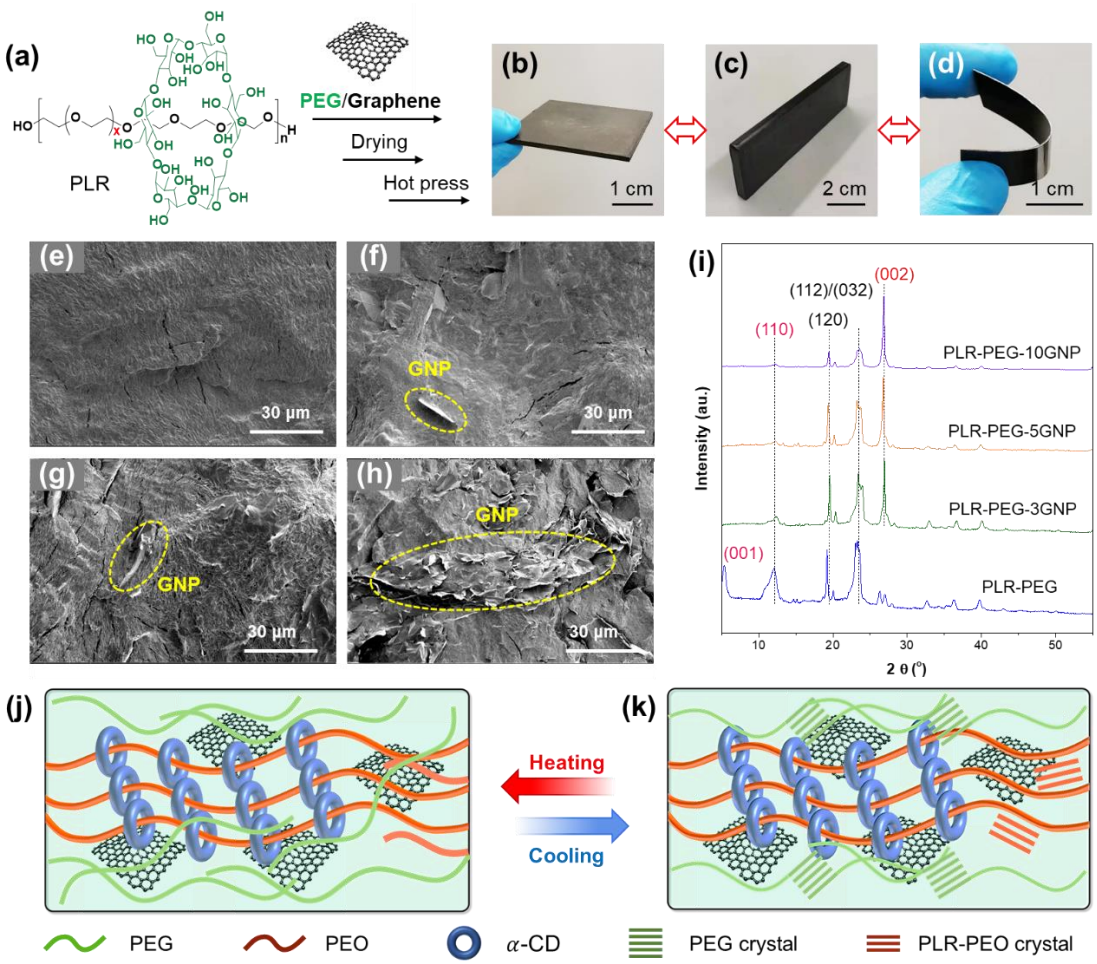

Figure 1. (a) Chemical structure of polyrotaxne and the three steps for PCM composites fabrication (namely, blending with PEG and GNP, freeze drying to remove the water, and hot press to obtain the samples with designed shapes), (b) sample with size of 50 mm ×50 mm ×2 mm, (c) sample with size of 100 mm × 50 mm ×5 mm, (d) sample with size of 50 mm ×20 mm ×1 mm, Images obtained from the SEM of the PCMs correspond to (e) PLR-PEG, (f) PLR-PEG-3GNP, (g) PLR-PEG-5GNP, (h) PLR-PEG-10GNP, (i) XRD curves of the four PCMs, (j) illustration of melting state of the PCM composites, and (k) diagram of crystalline state of the material at room temperature.

SEM micrographs of fractured surface of PLR-PEG nanocomposites containing GNPs are illustrated in **Figure 1e-h**. As shown in Figure 1e, the surface is relatively smooth, and we can observe a compact structure. With the introduce of GNP, we can see that the

surface becomes rougher with a higher content of GNPs. This roughness can be attributed to the well dispersion of GNPs in the PCM matrix, at least we can see it clearly in Figure 1f-h correspond to the percentages of 3 wt% and 5 wt% of GNPs. It is evident that certain GNP nanosheets are embedded in the PCM matrix but this nanosheets are well covered by the matrix, with no any obvious gaps (Figure 1f and g) between GNPs and matrix, which is evidence of the good compatibility between the PCM and GNP. We assigned this is an important reason why GNP can increase the crystallinity, which will be discussed in the following section.

As shown in **Figure 1h**, the surfaces are shown with a multitude of folds that are stacked layer by layer which may provide a lattice structure through which phonons can travel efficiently and enhance heat transfer, giving rise to a higher thermal conductivity, which will be discussed in *section 2.2*.

The X-ray diffractions (XRD) were shown in **Figure 1i**. We could see that all samples show two intense peaks at $2\theta \sim 19°$ and $2\theta \sim 23°$, which are attributed to crystal reflection planes (120) and concerted (112)/(032) planes of PEG, respectively, confirming the high degree of crystallinity of the structure. Furthermore, in the PCM reference pattern we observe two clear peaks at $2\theta = 5.4°$ (001) and 12.8° (110). [30] The latter (110) is also seen in the other samples but with less intensity. These peaks are obtained from the dried PLR crystal consisting of α-CD and PEO, this α-CD crystal can be maintained in a certain temperature range. Finally, in all samples containing GNPs, a very intense peak appears, which increases in intensity the higher the percentage of GNP in the samples. This peak is observed more or less at $2\theta \sim 26.4°$.[31] This peak corresponds to the crystallinity plane (002) of the GNPs. Finally, the melting and solid internal molecular structure illustrations are shown in **Figure 1j** and 1k. Typically, the GNPs are dispersed in the collective, and

the cyclodextrin crystal is well maintained within a certain temperature range, which acts as a physical crosslinking point.

2.2 Phase change behaviors

As a premise of the previous work, an important property of this PCM is the shape stability, which was already achieved thanks to the formalization of the polyrotaxane[19]. This property, which is partly due to good encapsulation ability, is also important for industrial application, especially when used in the thermal management of electronic devices, because PCM leakage not only reduces the thermal management efficiency, but also carries a risk to the operation of the equipment.[18] Therefore, we subject square samples of our PCM (20 mmx 20 mmx 3 mm) to a higher temperature than PEG 6K and PEO melting temperature [9]. In this case we will expose the samples to a temperature of 80°C for 1 h. The results can be seen in **Figure 2a**, where we can compare the photos at room temperature compared to those obtained after heat treatment. It can be clearly observed that there is no any leakage of PEG, and also maintains the initial shape without any obvious deformation, which directly confirmed the form stable and antileakage performances.

The heat conductivity in the PLR-PEG-GNPs were performed by using a thermal constants analyzer (TPS2500 S, Hot Disk) at room temperature with samples higher than 4 mm of thickness. The results were summarized in **Figure 2b**. The results for PLR-PEG, PLR-PEG-3GNP, PLR-PEG-5GNP and PLR-PEG-10GNP are as follows respectively: 0.30±0.05 W/(m·K), 0.48 ±0.07 W/(m·K), 0.78 ±0.05 W/(m·K) and 1.07 ±0.01 W/(m·K), corresponding to an increase of 60%, 160% and 257% respectively. High thermal conductivity is a significant property considered for the advanced thermal energy storage and heat transfer of PCMs. It is worth noting the synthesis processes are simple and green-

pathway, only in 3 steps and only using water as a solvent, which can ease the production cost to a certain extent from a commercial point of view.

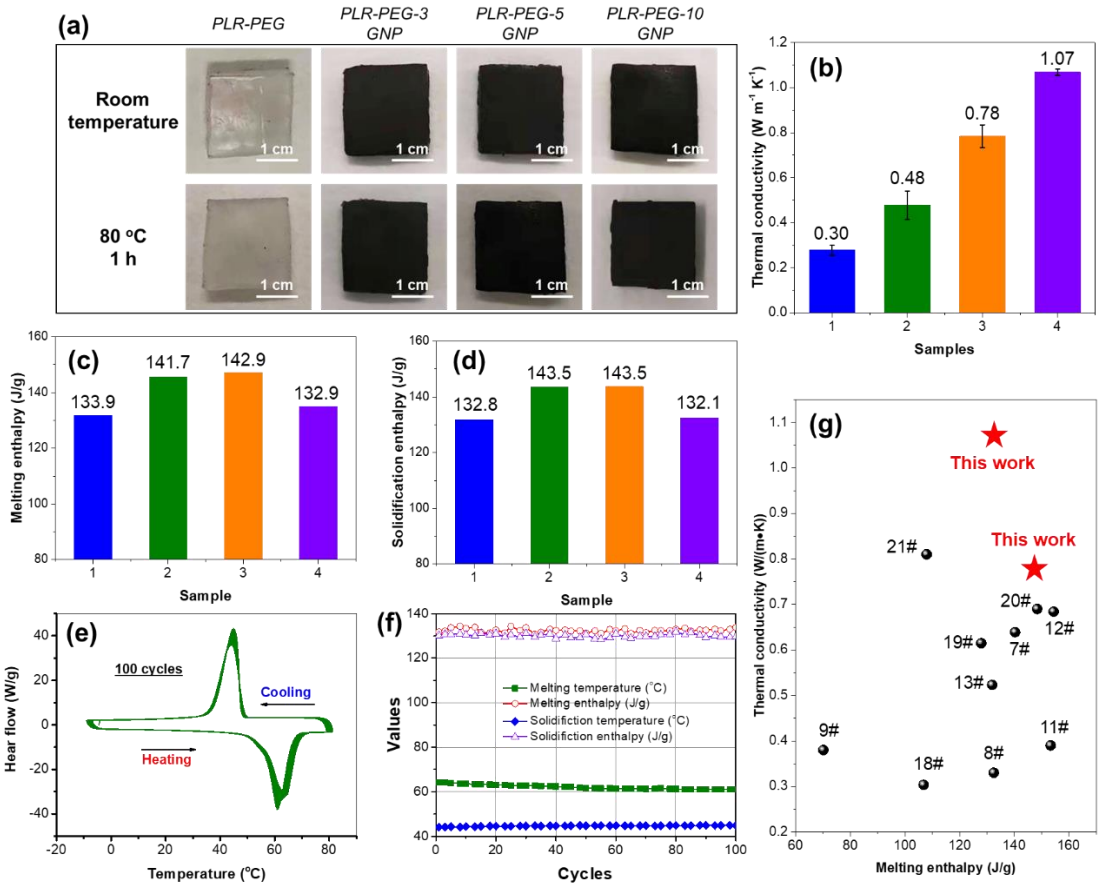

Figure 2. (a) Images of samples before and after heat treatment, (b) Thermal conductivity parameters of the samples, (c) graph with data of latent heat (ΔH_m (J/g)) and melting temperature T_s (ºC), (d) graph with data of solidification enthalpy (ΔH_s (J/g)) and solidification temperature T_s (ºC), (e) DSC curves during 100 cycles, (f) Plot of DSC parameters of solidification enthalpy (ΔHs (J/g)) and solidification temperature Ts (ºC), latent heat (ΔHm (J/g)) and melting temperature Ts (ºC) during the 100 cycles and (g) Comparation of ΔH_m and thermal conductivity with some typical values in recent report elsewhere.

202 **Table 1**. Comparison with the fabrication method, key parameters for the PEG based

203 PCMs in the recent reports elsewhere.

No.	**Supporter materials**	**Preparation method**	**PCM loading rate (%)**	**Enthalpy efficiency (%)**	**Latent heat (J g^{-1})**	**Thermal conductivity (W/(m·K))**	**References**
1	Poly (Glycerol-Itaconic acid)	Melting copolymerization	72.7	67.9	86.9	-	[32]
2	Vanadium dioxide	Vacuum impregnation	63.9	-	104.3	-	[33]
3	Graphene oxide and hexagonal boron nitride	Grafted polymerization	-	81.1	149.4	-	[34]
4	Toluene diisocyanate	Esterification	89.4	-	141.0	-	[35]
5	Melamine foam	Vacuum impregnation	68.5	56.3	148.9	-	[36]
6	Lamellar anhydrous calcium sulfate	Vacuum impregnation	-	93.0	93.5	-	[37]
7	Orange peel-based porous carbon	Vacuum maceration	-	88.0	140.3	0.6390	[38]
8	Silicon dioxide network with aminopropyl group and carboxylic	Sol-gel method	84.8	-	132.5	0.3300	[39]

	multi-walled carbon nanotubes						
9	Bio-based poly (glycerol-itaconic acid)	Solvent free	-	-	70.1	0.3800	[40]
10	Compounding polyethylene glycol and graphene oxide	Ultrasound-assisted physical blending	95.0	-	87.4	-	[41]
11	3D porous TiO_2	In situ encapsulate	92.0	-	153.3	0.3900	[42]
12	Calcium ion-crosslinked SA/kapok fiber aerogel	Vacuum impregnation	-	-	154.4	0.6840	[43]
13	Graphene oxide nanosheets modified with CoO nanoparticles	Physical mixing and melt impregnation method	80.2	99.8	131.9	0.5231	[44]
14	Hydroxy-terminated poly(dimethyl siloxane)	Condensation polymerization	99.0	63.9	124.5	-	[45]
15	Poly (butylene terephthalate)	Melting blend	91.0	83	136.8	-	[46]
16	Biomass porous potatoes	Vacuum impregnation	82.1	77.7	139.88	-	[47]

17	Cellulose nanofibers and carbon nanotubes	Crosslinking blending	90.0	99.25	158.3	-	[48]
18	4’4-diphenylmethane diisocyanate	Two-step solvent	-	74.8	106.8	0.3035	[49]
19	Hydroxylated carbon nanotubes	Chemical grafting	91.0	-	127.9	0.6147	[50]
20	Graphene oxide aerogel	Vacuum impregnation	96.4	-	148.4	0.6900	[51]
21	Carbon fiber/boron nitride-based nested structure	Melt blending	63.2	59.6	107.9	0.8100	[52]
22	Expanded vermiculite	Physical impregnation	74.9	-	139.2	-	[53]
23	Hydroxyapatite and dickite	Direct impregnation	74.7	-	153.5	-	[54]
24	PLR	Physical blending	60.0	115.4	147.2	0.78	This work

The phase change temperature and thermal energy storage properties of the PCM composites were measured by the DSC. The melting and solidifying DSC curves of the PLR-PEG GNP composites are shown in **Figure S1** to **S4**.

The detailed calorimetric results of the DSC experiments are listed in **Table S2**, including, end solidifying temperature ($T_{s\ onset}$), start melting temperature ($T_{m\ onset}$), peak

melting temperature ($T_{m,\ peak}$) and endothermic/exothermic enthalpy ($\Delta H_m/\Delta H_s$). The melting and solidification enthalpies are reflected in the graphs in **Figure 2**c and **d**. Notably, the melting enthalpy increased from 132.9 to 142.9 J/g. It also included values of for calculated enthalpy, Enthalpy efficiency, extent of supercooling values and crystallinity which we have already described how to do in the materials and methods section.

As shown in Table S2, Tm of the sample increases after adding GNP, indicating that GNP can promote PEG crystallization. This can also be proved in the calculation results of crystallinity. The crystallinity (φ_c%) were calculated based on the second heating by the following equation: [55]

$$\varphi_{c,PEG+PEO}\% = \frac{\Delta H_m}{\omega_{PEG+PEO}\Delta H_m^0} \times 100\% \quad (1)$$

where, ΔH_m was the measured enthalpy of melting, ΔH_m^0 was the melting enthalpy for a 100 % crystalline material and $\omega_{i,PEO+PEG}$ [%] was the fraction of the PEG and PEO in the sample. The ΔH_m^0 of PEO (or PEG) was 196.4 J g^{-1}.[56] As a result, the calculated crystallinity are 78.1%, 85.7%, 88.1%, and 85.9% for sample PLR-PEG, PLR-PEG-3GNP, PLR-PEG-5GNP and PLR-PEG-10GNP, respectively.

This occured because the GNPs can act as a nucleating agent, accelerating the nucleation of the PEG/PEO chains. This phenomenon can confirm the good dispersion in these samples to a certain extent, since the efficiency of a nucleating agent in the crystallization of a polymer depends very much on the dispersion of the agent in the polymer matrix. The more dispersed it is, the better it can interact with the polymer matrix chains.[57]

The extent of supercooling (ΔT, °C) was calculated by equation (2) [58]:

$$\Delta T = T_{m,onset} - T_{s,onset} \quad (2)$$

where, $T_{m,onset}$ [°C] is onset temperature of melting and $T_{s,onset}$[°C] is onset temperature

of crystallization. Based on equation (2), ΔT of the PCMs encapsulating PEG 6k are all calculated to be 9.2~11.3 ^{o}C, as listed in Table S2. The enthalpy efficiency (EE) of PCMs (PEG) can be determined by equation (4), [60]

$$EE\ \% = \frac{\Delta H_m}{\omega \Delta H_{PCM}} \times 100\ \% \quad (4)$$

where, ΔH_m [J g^{-1}] is the enthalpy value of the target PCMs. ΔH_{PCM} [J g^{-1}] represents the enthalpy of PCM substance, namely, PEG, and ω [%] is the mass ratio of PEG in the PCMs. Good values are maintained in the enthalpy efficiency, all above 100 % (The calculated values are listed in Table S2), which means that it does not have much heat loss during the cooling process, indicating that latent heat can be released during the cooling stage and increase the energy efficiency.

The extent of supercooling has no significant change, remaining around 10^{o}C. Although in the 3% and 5 % GNPs samples a slight increase is seen and this phenomenon may be because the GNPs influence the nucleation of the PEG/ PEO chains, making the degree of crystallinity also increase as we can see in the values of **Table S2**.

The large exposed surface area of GNPs can offer an improvement in nucleation during polymer crystallization. But first it is necessary to achieve a good GNP dispersion in the polymers. When with the low GNP, the GNP particles exhibit a strong nucleating effect and act as heterogeneous nucleation sites at the interfaces of the polymer with the GNP, but if this concentration increases, the presence of abundant GNP particles significantly hinders the diffusion of the polymer chains towards the growing crystallites, therefore, the crystallinity is reduced a little bit. That way when GNP reach 10 wt. % in our samples this effect is not so clear anymore, due to the graphene agglomerations in the structure, and at this time, the impurity effect of graphene has been revealed.

For latent heat thermal energy storage, a cyclic stability is very important because it translates into the useful life that the PCM will have for that application. To achieve that

propose, PCMs must be thermally stable over a large number of melting and cooling cycles. Therefore, we submitted one of the samples, PLR-PEG-10 GNP, to have 100 DSC cycles.

As we can see in **Figure 2**e and f, there is no significant change in any of the enthalpy and temperature values. This may also be due to the influence of GNPs due to the interactions between GNPs and PEG, such as surface tension forces, and capillary forces, will confine the flowability of PEG molecules, resulting in the decrease in phase change (melting) temperature.[61] This can occur because the GNP can reinforce its function throughout the cycles ensuring stability. Based on these results it can be concluded that the PLR-PEG-10GNP composite PCM showed excellent cycling performance (**Figure 2g**). Some other detailed method and key PCM parameters are summarized in Table 1.

2.3 Heat response

To see the thermal response and phase change behavior, we summit samples of the same size to a hot plate for heating and then cooling respectively. The IR images collected during the process can be seen in **Figure 3a**. The behavior of the PCM can be observed in the heating process, the sample is absorbing heat until it reaches the melting point with structure collapse, the phase change, and remains thermally stable until the phase change ends and continue absorbing heat, this phase change can be seen as a plateau in the curve (as shown in the red region in **Figure 3b**). The cooling process is the same, it goes down in temperature until it reaches its solidification temperature range, but here we can see the supercooling process (Region A, Figure 3c), due to the difference in melting and solidification temperatures it makes a rebound effect before entering the plateau. In addition, region A appears in the cooling process, which is also known as $T_{s,onset}$. The curve shows that the temperature rises at the initial stage of crystallization, which is due

285 to the exothermic crystallization with heat release to a certain extent, which leads to the
286 sample surface temperature increase.
287

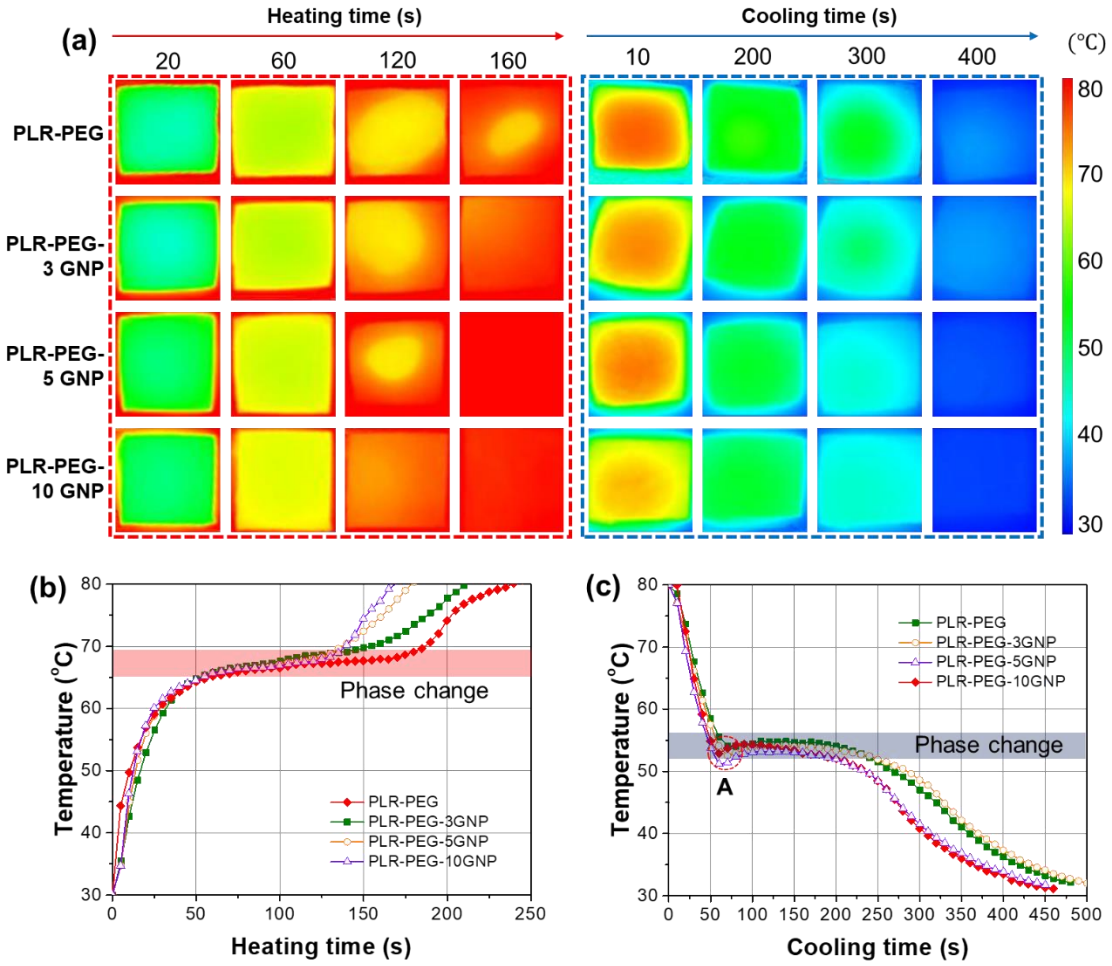

288

289 **Figure 3**. Heat response test: (a) Thermal images of the samples during heating and
290 cooling process (sample size: 20 mm×20 mm×3 mm), (b) the heating plots, and (c) the
291 cooling curves of the all samples.
292

293 The phase change during the heating process occurs between 60-70ºC and in the cooling
294 process between 55-50 ºC. There is an evident difference in temperature increasing rate
295 between PLR-PEG and GNP-containing samples. GNP containing samples behave the
296 relative fast thermal response rate of heating and cooling than the reference. The action
297 of GNP increases the thermal conductivity of the samples (As described in section 2.2).

This property is important for some applications that require a fast heat response (meaning fast charge or discharge of heat) like to thermal management of electronic devices or solar energy harvesting.

2.4 MCC testing and thermal stability

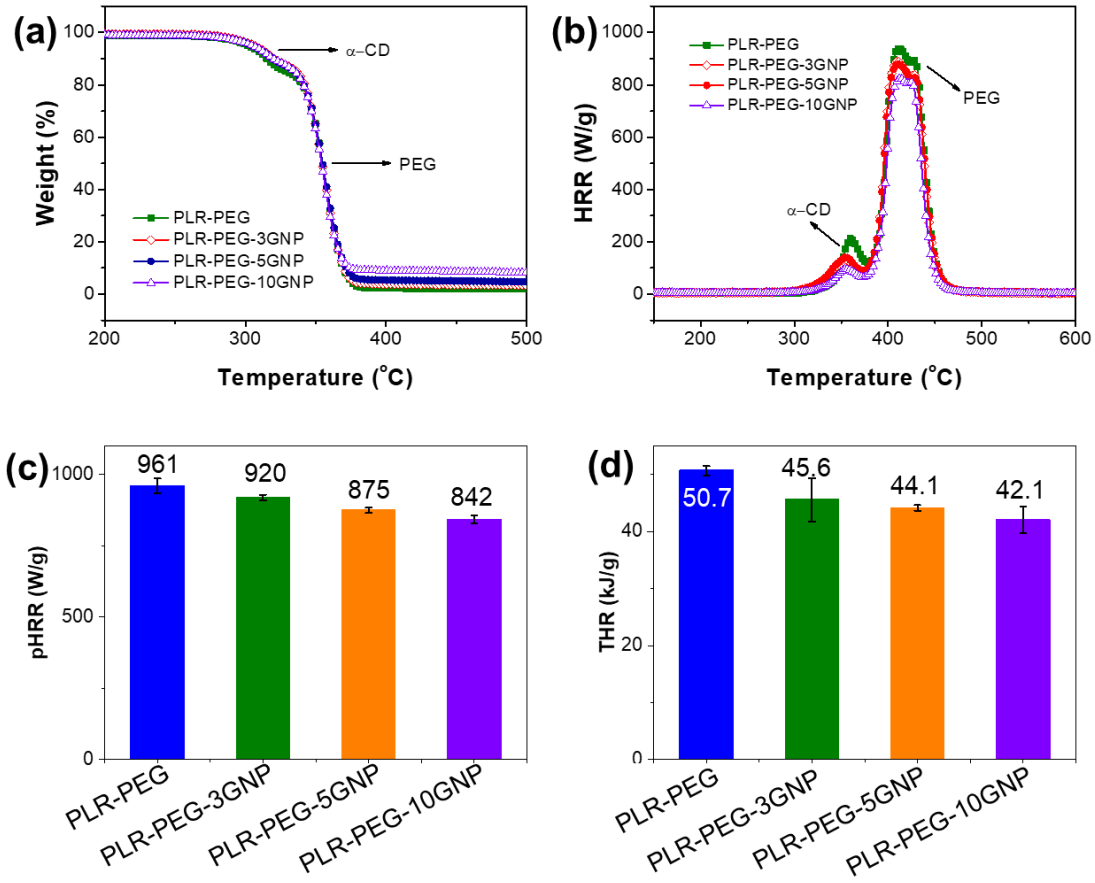

Figure 4. (a) TGA curves (N_2), (b) HRR curves of the four samples obtained by MCC, (c) Peak heat release (pHRR) data for all the samples, and (d) Total heat release (THR) data for all the samples.

Conversely thermal stability is a critical parameter for the melt-processing of polymers. The curves obtained with the TGA under N_2 atmosphere can be seen in **Figure 4a**, it can be noticed that the degradation occurs in two steps, the first one corresponding to approximately 9 wt %. of mass lose and it corresponds to the degradation of the α-CD at

311 ~310 °C. The second degradation occurs at ~350 °C and corresponds to the degradation
312 of the PEO or PEG.[62] We could see that more than 90 wt% of the samples are degraded,
313 the residue remaining in the samples with GNP, a percentage of residue in accordance
314 with the concentration of GNP in the PCM as it shown in **Table 2**. All the TGA results
315 indicated that the introduce of Graphene doesn´t influence the PLR-PEG thermal stability
316 significantly.

317 **Table 2**. TGA parameters and MCC results

Sample	**$T_{5\%}$ (°C)**	**T_{max1} (°C)**	**T_{max2} (°C)**	**Re.%**	**pHRR (W/g)**	**THR (kJ/g)**
PLR-PEG	303.1	315.1	357.1	2.0	961 ±25	50.7±0.8
PLR-PEG-3GNP	306.6	315.6	356.6	3.6	920±10	45.6±3.8
PLR-PEG-5GNP	304.9	316.2	356.8	5.7	875±9	44.1±0.5
PLR-PEG-10GNP	304.3	314.4	355.9	8.8	842±14	42.1±2.4

318

319 It is reported that GNPs can improve flame retardancy in polymer nanocomposites with
320 promising results.[63] The fire resistance in our samples was investigated using a micro
321 combustion calorimeter (MCC). This test is used to measure the heat released by materials
322 using small-scale oxygen consumption calorimetry, which is the main parameter for
323 evaluation of fire resistance, such as the peak heat release rate (pHRR, W/g) and the total
324 heat release (THR, KJ/g), which is the amount of heat released by the sample during
325 whole ignition process.

326 As we also saw in the TGA results previously, the PCM degradation here in MCC test

is done in two steps. The first peak that can be seen in **Figure 4b** belongs to the heat release due to the degradation of α-CD, while the largest peak corresponds to the degradation of PEG and PEO. All samples show the similar behavior. Thus, we could observe a HRR decrease in the two degradation peaks the higher the GNP content of the sample.

As shown in **Figure 4 b-d**, we can see a slight difference between the PLR- PEG reference and the samples with a content of GNPs, the decrease in the PHRR value and the total HR can be clearly seen the larger the percentage of GNPs, these decreases are 4.3-12.4% and 10.1-17.0% respectively. The great thermal conductivity that GNP possess makes a better distribute heat mixed with the formation of protective char layer formed by the GNPs which indicate a decrease in released heat due to the improved flame retardancy effect of GNPs in PLR-PEG matrix. It is worth pointing out that although GNP does not show significant catalytic effect on char formation, its two-dimensional nanostructure and good dispersion can act as a barrier for heat and mass conduction, thus having a positive effect on fire safety to a certain extent.

2.5 Application cases

2.5.1 Peak Shaving and Valley Filling for TEG

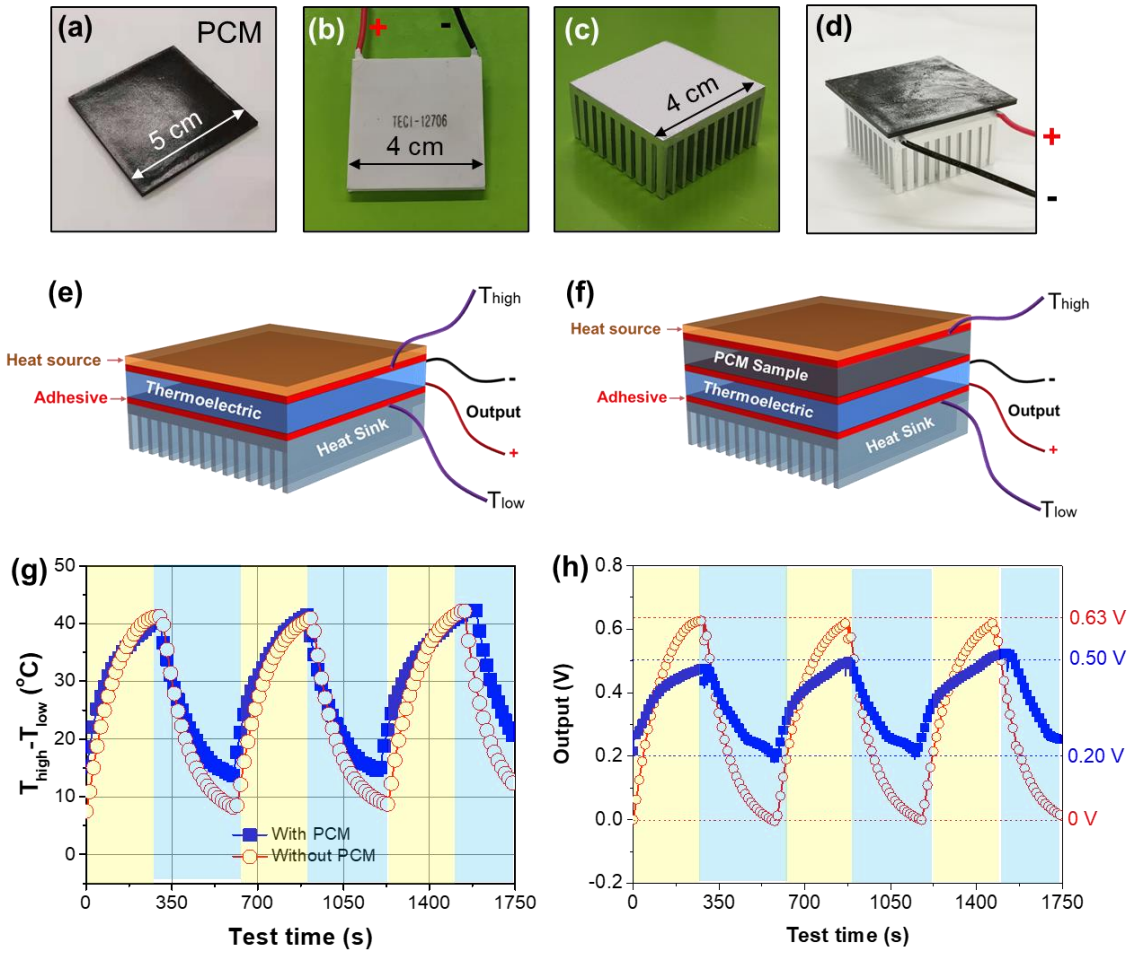

344

345 **Figure 5**. (a) PCM (sample PLR-PEG-5GNP) image (with size of 50 mm×50 mm×2 mm,
346 weight of 1.54 g), (b) TEG (Model: TECI-12706), (c) Heat sink, (d) schematic diagram
347 of test device, (e) structure illustration of the test devices without PCM, (f) Packed
348 structure illustration of device with PCM, (g) temperature difference of the two side of
349 TEG (T_{high} and T_{low}), and (h) Voltage output of the two devices with or without PCM.

350 With the temperature and heat absorb by the PCM, the heat response of the generator
351 can be delayed a little bit. Consequently, it performed as shown in the Figure 5g-h.
352 Fortunately, the output voltage can maintain 0.2 V while the sample without the PCM
353 will lose the output rapidly when removing the heat source. Advantage of PCM
354 incorporation make the output continuously and stably. It can be seen from **Figure 5g**
355 that the peak difference of temperature we control is almost the same. T_{high} is the heat

source temperature, and T_{Low} is the temperature at the interface between heat sink and thermoelectric converter. Due to the heat storage effect during PCM heating, the temperature difference is slightly larger after cooling. The system containing PCM in **Figure 5h** has significantly high peak output voltage. We believe that the important reason for this phenomenon is that during the limited heating cycle, the phase change of PCM will adjust the temperature difference on both sides of the thermoelectric converter. As a result, in the same heating cycle, the temperature difference is slightly lower than that of devices without PCM. Therefore, the peak value of the total voltage output is significantly lower than that of the sample without PCM. When the heat source is removed, PCM stores a certain amount of heat, which can fully serve as the heat source to maintain the temperature difference. Thus maintaining a relatively high voltage output during cooling, playing a significant practical effect of Peak Shaving and Valley Filling.

2.5.2 Solid state disc thermal regulation

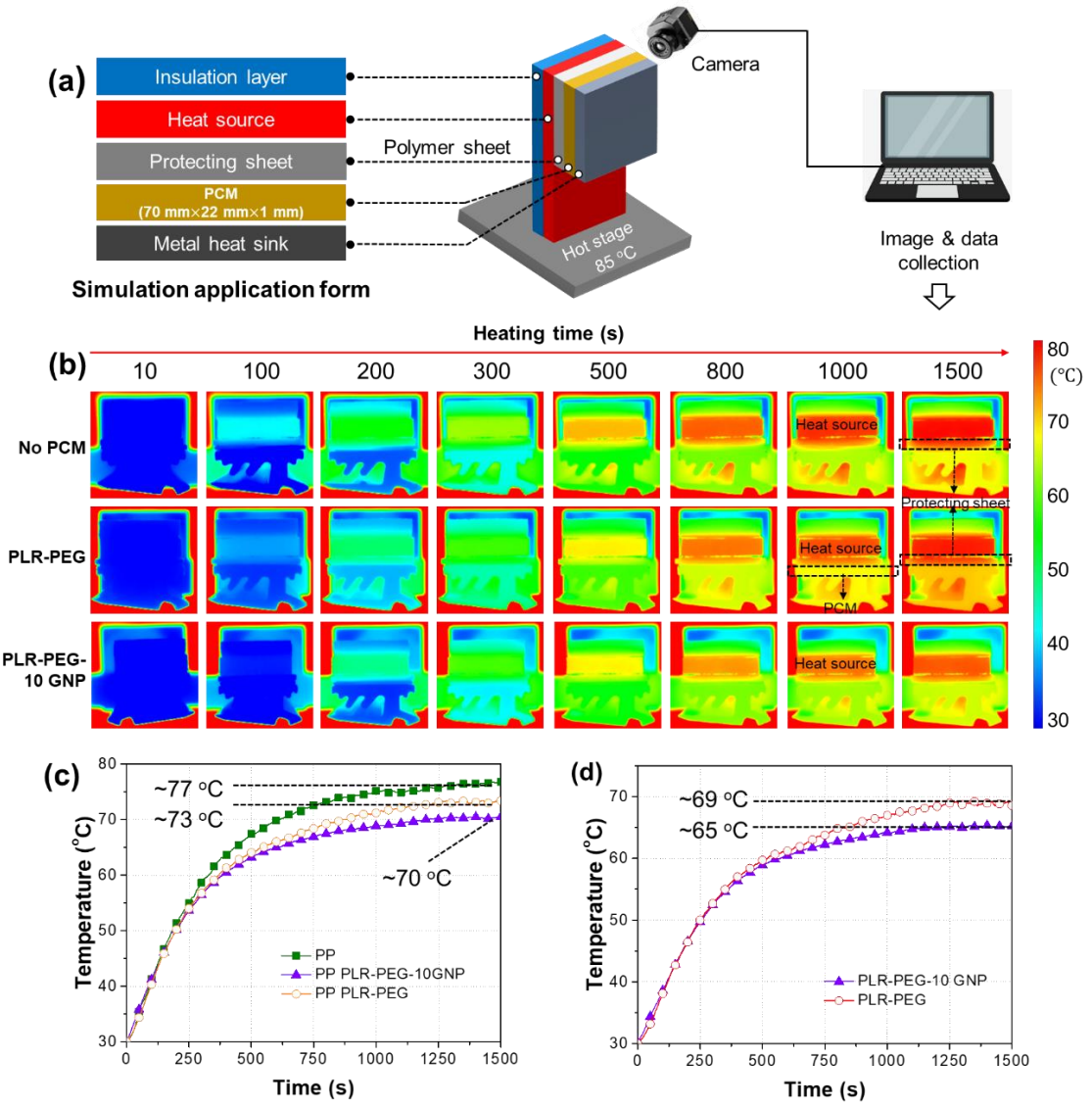

Figure 6. (a) Application form, and test diagram of the PCM for SSD thermal regulation, and illustration of the device stack structure, (b) IR images of the devices during heating, (c) the heating curves of the PP that without PCM, with sample PLR-PEG, and with PLR-PEG-10 GNP, and (d) heating curves of PCM layer with or without GNPs.

PCMs are usually used to regulate the temperature of solid-state disk (SSD). A schematic structure was designed (the protecting sheet (Polypropylene (PP) with 2 mm in thickness, PCM (70 mm×22 mm×1 mm in thickness, which is the same as the size of commercial product) as shown in **Figure 6a**. The IR images during heating was recorded and shown in **Figure 6b**. The corresponding plots were shown in **Figure 6c** and d. As it can be seen,

the endothermic and exothermic state of the device can form a relatively stable equilibrium temperature at last. During the whole heating cycle, sample with PCM in this study showed significantly better temperature control state than both the reference sample. Specifically, the temperature of the PP protecting part with PCM was significantly lower than that of blank sample. The temperature difference gradually appears and maintain between 4-7 ^{o}C for long period. The difference is due to the high enthalpy effect of both PLR-PEG and PLR-PEG-10GNP phase transition, which plays a role in temperature control for a certain period. We then found that PLR-PEG-10GNP sample has more excellent temperature control effect than PLR-PEG. We believe that this is due to the high thermal conductivity of PLR-PEG-10GNP. This will ensure efficient heat absorption and heat transfer, so as to give full play to the thermal management effect.

3. CONCLUSIONS

The PLR/PEG nanocomposites with various contents of GNPs were successfully prepared. Samples of PLR/PEG GNPs nanocomposites were fabricated using a blending method with water as the only solvent. The addition of GNPs to PLR / PEG maintained shape stability in its phase transition. Due to the good dispersion of GNP in the matrix in the concentrations 3 wt.% and 5 wt.% of GNPs we could see that it acts as a nucleating agent, slightly increasing the crystallinity and therefore the enthalpy values. A great thermal performance is observed, obtaining high latent heat values (132.9-142.9 J/g) and cyclical stability. We can further see a significant increase between 60-257 % compared to PLR-PEG in thermal conductivity, this increase is linear with the increase in GNP contents. It shows the improvement in fire resistance properties, lowering the values of pHRR and THR in a 4.3-12.4% and 10.1-17.0% respectively, and heat response, obtaining faster heating and cooling rates. For the application cases, it showed obvious Peak Shaving and Valley Filling and heat regulation for the SSD. To summarize, the high

thermal performance with high enthalpy values, the high thermal conductivity values, added the great form stability so that we obtain in PLR / PEG GNP, thus its simple synthesis process and green pathway to enhance the fire safety, make an optimal PCM to be used as an in latent heat thermal energy storage material in industrial applications such as device thermoregulator or thermoelectric generator.

Acknowledgment

The authors acknowledge the financial support provided by BIOFIRESAFE Project funded by Ministerio De Ciencia E Innovación (MINECO), Spain with Project number: PID2020-117274RB-I00BIOFIRESAFE.

4. REFERENCES

1. Debich, B.; El Hami, A.; Yaich, A.; Gafsi, W.; Walha, L.; Haddar, M., An efficient reliability-based design optimization study for PCM-based heat-sink used for cooling electronic devices. *Mechanics of Advanced Materials and Structures* **2022,** *29* (12), 1661-1673.
2. Kannan, K. G.; Kamatchi, R., Augmented heat transfer by hybrid thermosyphon assisted thermal energy storage system for electronic cooling. *Journal of Energy Storage* **2020,** *27*, 101146.
3. Sundararajan, S.; Samui, A. B.; Kulkarni, P. S., Versatility of polyethylene glycol (PEG) in designing solid–solid phase change materials (PCMs) for thermal management and their application to innovative technologies. *Journal of Materials Chemistry A* **2017,** *5* (35), 18379-18396.
4. Demirbas, M. F., Thermal Energy Storage and Phase Change Materials: An Overview. *Energy Sources, Part B: Economics, Planning, and Policy* **2006,** *1* (1), 85-95.
5. Souayfane, F.; Fardoun, F.; Biwole, P.-H., Phase change materials (PCM) for cooling applications in buildings: A review. *Energy and Buildings* **2016,** *129*, 396-431.
6. Javadi, F. S.; Metselaar, H. S. C.; Ganesan, P., Performance improvement of solar thermal systems integrated with phase change materials (PCM), a review. *Solar Energy* **2020,** *206*, 330-352.
7. Gharbi, S.; Harmand, S.; Jabrallah, S. B., Experimental comparison between different configurations of PCM based heat sinks for cooling electronic components. *Applied Thermal Engineering* **2015,** *87*, 454-462.
8. Sarier, N.; Onder, E., Organic phase change materials and their textile applications: An overview. *Thermochimica Acta* **2012,** *540*, 7-60.

9. Aftab, W.; Huang, X.; Wu, W.; Liang, Z.; Mahmood, A.; Zou, R., Nanoconfined phase change materials for thermal energy applications. *Energy & Environmental Science* **2018,** *11* (6), 1392-1424.
10. Yin, G.-Z.; Hobson, J.; Duan, Y.; Wang, D.-Y., Polyrotaxane: New generation of sustainable, ultra-flexible, form-stable and smart phase change materials. *Energy Storage Materials* **2021,** *40*, 347-357.
11. Chen, R.; Yao, R.; Xia, W.; Zou, R., Electro/photo to heat conversion system based on polyurethane embedded graphite foam. *Applied Energy* **2015,** *152*, 183-188.
12. Yuan, P.; Zhang, P.; Liang, T.; Zhai, S., Effects of surface functionalization on thermal and mechanical properties of graphene/polyethylene glycol composite phase change materials. *Applied Surface Science* **2019,** *485*, 402-412.
13. Jiang, Y.; Wang, Z.; Shang, M.; Zhang, Z.; Zhang, S., Heat collection and supply of interconnected netlike graphene/polyethyleneglycol composites for thermoelectric devices. *Nanoscale* **2015,** *7* (25), 10950-10953.
14. Sundararajan, S.; Samui, A. B.; Kulkarni, P. S., Interpenetrating phase change polymer networks based on crosslinked polyethylene glycol and poly(hydroxyethyl methacrylate). *Solar Energy Materials and Solar Cells* **2016,** *149*, 266-274.
15. Sarier, N.; Onder, E., The manufacture of microencapsulated phase change materials suitable for the design of thermally enhanced fabrics. *Thermochimica Acta* **2007,** *452* (2), 149-160.
16. Ding, E.-Y.; Jiang, Y.; Li, G.-K., COMPARATIVE STUDIES OF THE STRUCTURES AND TRANSITION CHARACTERISTICS OF CELLULOSE DIACETATE MODIFIED WITH POLYETHYLENE GLYCOL PREPARED BY CHEMICAL BONDING AND PHYSICAL BLENDING METHODS*. *Journal of Macromolecular Science, Part B* **2001,** *40* (6), 1053-1068.
17. Şentürk, S. B.; Kahraman, D.; Alkan, C.; Gökçe, İ., Biodegradable PEG/cellulose, PEG/agarose and PEG/chitosan blends as shape stabilized phase change materials for latent heat energy storage. *Carbohydrate Polymers* **2011,** *84* (1), 141-144.
18. Wei, X.; Jin, X.-z.; Zhang, N.; Qi, X.-d.; Yang, J.-h.; Zhou, Z.-w.; Wang, Y., Constructing cellulose nanocrystal/graphene nanoplatelet networks in phase change materials toward intelligent thermal management. *Carbohydrate Polymers* **2021,** *253*, 117290.
19. Yang, J.; Qi, G.-Q.; Liu, Y.; Bao, R.-Y.; Liu, Z.-Y.; Yang, W.; Xie, B.-H.; Yang, M.-B., Hybrid graphene aerogels/phase change material composites: Thermal conductivity, shape-stabilization and light-to-thermal energy storage. *Carbon* **2016,** *100*, 693-702.
20. Fan, X.; Liu, L.; Jin, X.; Wang, W.; Zhang, S.; Tang, B., MXene Ti3C2Tx for phase change composite with superior photothermal storage capability. *Journal of Materials Chemistry A* **2019,** *7* (23), 14319-14327.
21. Xue, F.; Jin, X.-z.; Xie, X.; Qi, X.-d.; Yang, J.-h.; Wang, Y., Constructing reduced graphene oxide/boron nitride frameworks in melamine foam towards synthesizing phase change materials applied in thermal management of microelectronic devices. *Nanoscale* **2019,** *11* (40), 18691-18701.
22. Chen, X.; Gao, H.; Yang, M.; Dong, W.; Huang, X.; Li, A.; Dong, C.; Wang, G., Highly graphitized 3D network carbon for shape-stabilized composite PCMs with superior thermal energy harvesting. *Nano Energy* **2018,** *49*, 86-94.
23. Potts, J. R.; Dreyer, D. R.; Bielawski, C. W.; Ruoff, R. S., Graphene-based polymer nanocomposites. *Polymer* **2011,** *52* (1), 5-25.
24. Silakhori, M.; Fauzi, H.; Mahmoudian, M. R.; Metselaar, H. S. C.; Mahlia, T. M. I.; Khanlou, H. M., Preparation and thermal properties of form-stable phase change

materials composed of palmitic acid/polypyrrole/graphene nanoplatelets. *Energy and Buildings* **2015,** *99*, 189-195.
25. Yavari, F.; Fard, H. R.; Pashayi, K.; Rafiee, M. A.; Zamiri, A.; Yu, Z.; Ozisik, R.; Borca-Tasciuc, T.; Koratkar, N., Enhanced Thermal Conductivity in a Nanostructured Phase Change Composite due to Low Concentration Graphene Additives. *The Journal of Physical Chemistry C* **2011,** *115* (17), 8753-8758.
26. Xue, S.; Lei, C.; Liu, D.; Wang, K.; Wu, K.; Fu, Q., Thermo-conductive phase change materials with binary fillers of core-shell-like distribution. *Composites Part A: Applied Science and Manufacturing* **2021,** *144*, 106326.
27. Cataldi, P.; Athanassiou, A.; Bayer, I. S., Graphene Nanoplatelets-Based Advanced Materials and Recent Progress in Sustainable Applications. *Applied Sciences* **2018,** *8* (9), 1438.
28. Ghasemi, I.; Gomari, S., Polymeric Nanocomposites Including Graphene Nanoplatelets. In *Handbook of Graphene Set*, 2019; pp 481-515.
29. Pereira, P.; Ferreira, D. P.; Araújo, J. C.; Ferreira, A.; Fangueiro, R., The Potential of Graphene Nanoplatelets in the Development of Smart and Multifunctional Ecocomposites. *Polymers* **2020,** *12* (10), 2189.
30. Uenuma, S.; Maeda, R.; Yokoyama, H.; Ito, K., Formation of Isolated Pseudo-Polyrotaxane Nanosheet Consisting of α-Cyclodextrin and Poly(ethylene glycol). *Macromolecules* **2019,** *52* (10), 3881-3887.
31. Chieng, B. W.; Ibrahim, N. A.; Yunus, W. M. Z. W.; Hussein, M. Z., Poly(lactic acid)/Poly(ethylene glycol) Polymer Nanocomposites: Effects of Graphene Nanoplatelets. *Polymers* **2014,** *6* (1), 93-104.
32. Yin, G.-Z.; Díaz Palencia, J. L.; Wang, D.-Y., Fully bio-based Poly (Glycerol-Itaconic acid) as supporter for PEG based form stable phase change materials. *Composites Communications* **2021,** *27*, 100893.
33. Bai, K.; Li, C.; Xie, B.; Zhang, D.; Lv, Y.; Xiao, J.; He, M.; Zeng, X.; Zeng, J.; Chen, J., Emerging PEG/VO2 dual phase change materials for thermal energy storage. *Solar Energy Materials and Solar Cells* **2022,** *239*, 111686.
34. Jing, R.; Zhang, H.; Huang, C.; Su, F.; Wu, B.; Sun, Z.; Xu, F.; Sun, L.; Xia, Y.; Peng, H.; Lin, X.; Li, B.; Zou, Y.; Chu, H.; Huang, P.; Yan, E., Construction of double cross-linking PEG/h-BN@GO polymeric energy-storage composites with high structural stability and excellent thermal performances. *Colloids and Surfaces A: Physicochemical and Engineering Aspects* **2022,** *638*, 128193.
35. Zhao, Y.; Liu, T.; Wei, Z.; Zhao, S.; Lei, J.; Fu, X., Towards high performance semi-interpenetrating phase change materials networks via linear polyethylene glycol-based multimerization effect. *Chemical Engineering Journal* **2022,** *446*, 136982.
36. Xiao, Y.-y.; He, Y.-j.; Wang, R.-q.; Lei, Y.-z.; Yang, J.-h.; Qi, X.-d.; Wang, Y., Mussel-inspired strategy to construct 3D silver nanoparticle network in flexible phase change composites with excellent thermal energy management and electromagnetic interference shielding capabilities. *Composites Part B: Engineering* **2022,** *239*, 109962.
37. Lou, J.; Zhang, K.; Qin, S.; Lei, Y.; Liu, Y.; He, M.; Yu, J., Two-dimensional lamellar phosphogypsum/polyethylene glycol composite PCM: Fabrication and characterization. *Journal of Industrial and Engineering Chemistry* **2022,** *113*, 431-438.
38. Xiao, S.; Zou, M.; Xie, Y.; Chen, W.; Hu, X.; Ma, Y.; Zu, S.; Che, Y.; Jiang, X., Nanosilver modified navel orange peel foam/polyethylene glycol composite phase change materials with improved thermal conductivity and photo-thermal conversion efficiency. *Journal of Energy Storage* **2022,** *56*, 105976.
39. Yan, D.; Ming, W.; Liu, S.; Yin, G.; Zhang, Y.; Tang, B.; Zhang, S., Polyethylene glycol (PEG)/silicon dioxide grafted aminopropyl group and carboxylic

multi-walled carbon nanotubes (SAM) composite as phase change material for light-to-heat energy conversion and storage. *Journal of Energy Storage* **2021,** *36*, 102428.
40. Yin, G.-Z.; Yang, X.-M.; Hobson, J.; López, A. M.; Wang, D.-Y., Bio-based poly (glycerol-itaconic acid)/PEG/APP as form stable and flame-retardant phase change materials. *Composites Communications* **2022,** *30*, 101057.
41. Li, M.; Wang, C., Preparation and characterization of GO/PEG photo-thermal conversion form-stable composite phase change materials. *Renewable Energy* **2019,** *141*, 1005-1012.
42. Sun, X.; Yi, M.; Feng, B.; Liu, R.; Sun, L.; Zhai, L.; Cao, H.; Zou, C., Shape-stabilized composite phase change material PEG@TiO2 through in situ encapsulation of PEG into 3D nanoporous TiO2 for thermal energy storage. *Renewable Energy* **2021,** *170*, 27-37.
43. Zhang, Q.; Chen, B.; Wu, K.; Nan, B.; Lu, M.; Lu, M., PEG-filled kapok fiber/sodium alginate aerogel loaded phase change composite material with high thermal conductivity and excellent shape stability. *Composites Part A: Applied Science and Manufacturing* **2021,** *143*, 106279.
44. Li, Y.; Li, Y.; Huang, X.; Zheng, H.; Lu, G.; Xi, Z.; Wang, G., Graphene-CoO/PEG composite phase change materials with enhanced solar-to-thermal energy conversion and storage capacity. *Composites Science and Technology* **2020,** *195*, 108197.
45. Sundararajan, S.; Samui, A. B.; Kulkarni, P. S., Crosslinked polymer networks of poly(ethylene glycol) (PEG) and hydroxyl terminated poly(dimethyl siloxane) (HTPDMS) as polymeric phase change material for thermal energy storage. *Solar Energy* **2019,** *181*, 187-194.
46. Yan, D.; Zhao, S.; Ge, C.; Gao, J.; Gu, C.; Fan, Y., PBT/adipic acid modified PEG solid-solid phase change composites. *Journal of Energy Storage* **2022,** *52*, 104753.
47. Fang, Y.; Liu, S.; Li, X.; Hu, X.; Wu, H.; Lu, X.; Qu, J., Biomass porous potatoes/MXene encapsulated PEG-based PCMs with improved photo-to-thermal conversion capability. *Solar Energy Materials and Solar Cells* **2022,** *237*, 111559.
48. Liu, Y.; Liu, H.; Qi, H., High efficiency electro- and photo-thermal conversion cellulose nanofiber-based phase change materials for thermal management. *Journal of Colloid and Interface Science* **2023,** *629*, 478-486.
49. Gao, N.; Tang, T.; Xiang, H.; Zhang, W.; Li, Y.; Yang, C.; Xia, T.; Liu, X., Preparation and structure-properties of crosslinking organic montmorillonite/polyurethane as solid-solid phase change materials for thermal energy storage. *Solar Energy Materials and Solar Cells* **2022,** *244*, 111831.
50. Yang, Y.; Yin, Q.; Xu, F.; Sun, L.; Xia, Y.; Guan, Y.; Liao, L.; Zhou, T.; Lao, J.; Wang, Y.; Wang, Y.; Song, L.; Li, D., Fabricated Polyethylene glycol/ hydroxylated carbon nanotubes shape-stabilized phase change materials with improving thermal conductivity. *Thermochimica Acta* **2022,** *718*, 179363.
51. Bao, Z.; Bing, N.; Yao, H.-R.; Zhang, Y.; Xie, H.; Yu, W., Three-Dimensional Interpenetrating Network Phase-Change Composites with High Photothermal Conversion and Rapid Heat Storage and Release. *ACS Applied Energy Materials* **2021,** *4* (8), 7710-7720.
52. Gong, S.; Li, X.; Sheng, M.; Liu, S.; Zheng, Y.; Wu, H.; Lu, X.; Qu, J., High Thermal Conductivity and Mechanical Strength Phase Change Composite with Double Supporting Skeletons for Industrial Waste Heat Recovery. *ACS Applied Materials & Interfaces* **2021,** *13* (39), 47174-47184.
53. Song, S.; Yang, Z.; Li, J.; Wang, C.; Zhao, S., Analysis and Optimization of Thermophysical Properties and Phase Change Behavior of Expanded Vermiculite-

Based Organic Composite Phase Change Materials. *Energy & Fuels* **2021,** *35* (3), 2727-2741.
54. Zheng, F.; Wang, C.; Huang, K.; Li, J., Surface Adsorption in PEG/Hydroxyapatite and PEG/Dickite Composite Phase Change Materials. *Energy & Fuels* **2021,** *35* (13), 10850-10859.
55. Yin, G.; Zhao, D.; Wang, X.; Ren, Y.; Zhang, L.; Wu, X.; Nie, S.; Li, Q., Bio-compatible poly(ester-urethane)s based on PEG-PCL-PLLA copolymer with tunable crystallization and bio-degradation properties. *RSC Advances* **2015,** *5* (96), 79070-79080.
56. Chrissopoulou, K.; Andrikopoulos, K. S.; Fotiadou, S.; Bollas, S.; Karageorgaki, C.; Christofilos, D.; Voyiatzis, G. A.; Anastasiadis, S. H., Crystallinity and Chain Conformation in PEO/Layered Silicate Nanocomposites. *Macromolecules* **2011,** *44* (24), 9710-9722.
57. Broda, J.; Baczek, M.; Fabia, J.; Binias, D.; Fryczkowski, R., Nucleating agents based on graphene and graphene oxide for crystallization of the β-form of isotactic polypropylene. *Journal of Materials Science* **2020,** *55* (4), 1436-1450.
58. Zhang, X.; Liu, H.; Huang, Z.; Yin, Z.; Wen, R.; Min, X.; Huang, Y.; Liu, Y.; Fang, M.; Wu, X., Preparation and characterization of the properties of polyethylene glycol @ Si3N4 nanowires as phase-change materials. *Chemical Engineering Journal* **2016,** *301*, 229-237.
59. Jackson, C. L.; McKenna, G. B., The melting behavior of organic materials confined in porous solids. *The Journal of Chemical Physics* **1990,** *93* (12), 9002-9011.
60. Cheng, P.; Gao, H.; Chen, X.; Chen, Y.; Han, M.; Xing, L.; Liu, P.; Wang, G., Flexible monolithic phase change material based on carbon nanotubes/chitosan/poly(vinyl alcohol). *Chemical Engineering Journal* **2020,** *397*, 125330.
61. He, L.; Wang, H.; Zhu, H.; Gu, Y.; Li, X.; Mao, X., Thermal Properties of PEG/Graphene Nanoplatelets (GNPs) Composite Phase Change Materials with Enhanced Thermal Conductivity and Photo-Thermal Performance. *Applied Sciences* **2018,** *8* (12), 2613.
62. Yin, G.-Z.; Zhou, M.-H.; García, M. F. A.; Rincón Arévalo, P., Surface grafting POSS to improve the hydrophobicity and fire safety of Polyrotaxane based smart phase change materials. *Advanced Industrial and Engineering Polymer Research* **2023**.
63. Inuwa, I. M.; Hassan, A.; Wang, D.-Y.; Samsudin, S. A.; Mohamad Haafiz, M. K.; Wong, S. L.; Jawaid, M., Influence of exfoliated graphite nanoplatelets on the flammability and thermal properties of polyethylene terephthalate/polypropylene nanocomposites. *Polymer Degradation and Stability* **2014,** *110*, 137-148.